AAS 19-466

DISPOSAL, DEPLOYMENT, AND DEBRIS IN NEAR RECTILINEAR HALO ORBITS

Diane C. Davis,[*] Kenza K. Boudad,[†] Sean M. Phillips,[‡] and Kathleen C. Howell[§]

A proposed Gateway facility in a lunar Near Rectilinear Halo Orbit (NRHO) will serve as an outpost in deep space, with spacecraft periodically arriving and departing. Departing objects will include logistics modules, requiring safe disposal; cubesats, deployed to various destinations; and debris objects, whose precise paths may be unknown. Escape dynamics from NRHOs are complex; motion is primarily influenced by the Earth and Moon within the orbit, but spacecraft are significantly impacted by solar gravity upon departure. The current investigation explores the dynamics of departure from the NRHO, including the risk of debris recontact, safe heliocentric disposal, and deployment to select destinations.

INTRODUCTION

The Lunar Orbital Platform-Gateway[1] is proposed as an outpost in deep space: a proving ground for deep space technologies and a staging location for missions beyond Earth orbit. Envisioned as a crew-tended spacecraft, the Gateway will be constructed over time as various components are delivered either as co-manifested payloads with Orion or independently without crew presence. Naturally, spacecraft and objects with a wide range of shapes and masses will also depart the Gateway for other destinations. Examples of Gateway departures are wide ranging and include fast, crewed transits back to Earth, deployment of cubesats to locations in cislunar space, departure for Mars, lander descent to the lunar surface, safe disposal of discarded logistics modules to heliocentric space, deployment of servicing spacecraft to satellites in Sun-Earth halo orbits, and venting of wastewater into space. Each of these examples represents an object departing the Gateway under varying circumstances; each departure is governed by the dynamics of the Gateway orbit and the surrounding dynamical environment.

The current baseline orbit for the Gateway is a Near Rectilinear Halo Orbit (NRHO) near the Moon.[2] Two NRHOs are investigated in the current analysis; both exhibit nearly-stable behavior, but over time, any unmaintained object in such an orbit eventually departs due to the small instabilities associated with these NRHOs. A separation maneuver speeds the departure from the NRHO, but the effects of the maneuver on the spacecraft behavior depend on the location, magnitude, and direction of the burn. A previous investigation[3] examined departure from the NRHO and escape from the Earth-Moon vicinity from the perspective of logistics module (LM) disposal. The current investigation extends this work, exploring several additional aspects of the dynamics of departure from the NRHO. The analysis is applicable to large Gateway components like the LM, small cubesats, and particles in frozen wastewater plumes. The first phase of the

[*] Principal Systems Engineer, a.i. solutions, Inc., 2224 Bay Area Blvd, Houston TX 77058, diane.davis@ai-solutions.com.
[†] Graduate Student, School of Aeronautics and Astronautics, Purdue University, Armstrong Hall of Engineering, 701 W. Stadium Ave., West Lafayette, IN 47907-2045, kboudad@purdue.edu.
[‡] Principal Software Engineer, a.i. solutions, Inc., 4500 Forbes Blvd., Lanham MD 20706, sean.phillips@ai-solutions.com.
[§] Hsu Lo Distinguished Professor, School of Aeronautics and Astronautics, Purdue University, Armstrong Hall of Engineering, 701 W. Stadium Ave., West Lafayette, IN 47907-2045, howell@purdue.edu. Fellow AAS; Fellow AIAA.

analysis addresses immediate post-separation behavior. After separation from the Gateway, a departing object may diverge from the NRHO immediately, or it may remain in the vicinity of the NRHO for one or many revolutions. The rate of departure depends on the location, magnitude, and direction of the separation Δv. Some maneuvers result in trajectories that risk recontacting the Gateway, leading to collision or contamination concerns. The extensive magnitude of the design space leads to computational complexity, and recontact maps are generated to facilitate the analysis. In the second phase of the study, the path of the spacecraft ix examined once it is no longer near the Gateway. After a spacecraft has departed the NRHO, the dynamics are dominated by the gravity of the Sun and Earth, and the flow of trajectories in the multibody regime governs its eventual destination.

DYNAMICAL MODELS

In this investigation, three dynamical models are employed. The Circular Restricted 3-Body Problem (CR3BP)[4] provides a framework for investigation of departure dynamics and flow nearby the NRHO before and immediately after separation from the Gateway. In this regime, the primary gravitational influences on the spacecraft are the Earth and Moon, and the CR3BP is an effective approximation for the dynamics. As the spacecraft departs the immediate vicinity of the NRHO, the effects of the Sun become significant. Thus, the Bicircular Restricted 4-Body Problem (BCR4BP)[5] is employed to characterize the behavior of the departing spacecraft. The BCR4BP incorporates the influence of solar gravity on the Earth-Moon-spacecraft three-body system and offers an increase in fidelity over the CR3BP, while still offering insight into the underlying dynamical behavior in the system. Finally, an N-body model based on ephemeris data provides higher fidelity analysis for particular mission scenarios.

The Circular Restricted 3-Body Problem

The CR3BP describes the motion of a massless spacecraft affected by two primary gravitational bodies such as the Earth and the Moon. The model assumes that the two primary bodies are point masses orbiting their center of mass in circular orbits. The spacecraft moves freely under the influence of the two primaries, and its motion is described relative to a rotating reference frame. No closed-form solution exists to the CR3BP equations of motion, but five equilibrium solutions, the libration points, are denoted L_1 through L_5. Stable and unstable periodic orbit families, including the L_2 halo orbits, emerge in the vicinity of the libration points. A single integral of the motion exists in the CR3BP. An energy-like quantity, the Jacobi constant limits the motion of the spacecraft to regions in space where $v^2 > 0$, with zero velocity surfaces (ZVSs) bounding the regions within which the spacecraft can move freely. For values of Jacobi constant greater than that associated with the L_1 libration point, the ZVSs form closed regions around each of the two primaries. As the energy of the spacecraft trajectory increases, the value of Jacobi constant decreases until, at the L_1 value, the ZVSs open at the L_1 libration point and the spacecraft can move between the two primaries. Similarly, when the value of the Jacobi constant decreases to the value associated with L_2, the ZVSs open at L_2 and the spacecraft is able to escape the vicinity of the primaries entirely. For spacecraft orbiting in one of the selected NRHOs, the CR3BP is a good approximation for the behavior of the trajectory.

The Bicircular Restricted 4-Body Problem

As the spacecraft begins to depart the NRHO, the gravitational influence of the Sun becomes non-negligible, and a higher fidelity model is necessary to accurately describe spacecraft behavior. The BCR4BP incorporates the gravitational effect of three massive bodies, for instance, the Earth, the Moon and the Sun, on the motion of a spacecraft *P*. The mass of the spacecraft is assumed to be negligible in comparison to the masses of the other bodies. As illustrated in Figure 1, the Earth and the Moon are assumed to move in circular orbits around their common barycenter, denoted B_1, while the Sun and B_1 move in circular orbits with respect to the Earth-Moon-Sun barycenter, labelled B_2. In addition to the inertial frame, two rotating frames are defined. An Earth-Moon (E-M) rotating frame is fixed with the $\hat{x}$ axis lying along the Earth-Moon line, the $\hat{z}$ axis aligned with primaries' orbital angular momentum, and the $\hat{y}$ axis completing the right-handed orthonormal set. The solar orbital plane is defined by the inclination i with respect to the Earth-Moon plane and the longitude Ω of the Sun ascending node along its orbit. As observed in Figure 1, the second rotating frame, S-B_1 is fixed with respect to the motion of the Sun and B_1, the Earth-Moon barycenter. The $\hat{x}'$ axis is defined along the line joining the Sun to B_1, $\hat{z}'$ is aligned with the Sun - B_1 angular momentum vector, and

$\hat{y}'$ completes the right-handed orthornomal set. The position of the Sun as viewed in the Earth-Moon rotating frame is denoted the Sun angle, defined as the angle between the rotating $\hat{x}$ axis and the Sun position vector. Since the Sun orbit is circular in the BCR4BP, the Sun angle is a linear function of the time, $\theta_S = \omega_S\, t + \theta_{S0}$, where ω_S is the angular velocity of the Sun rotation, as viewed in the Earth-Moon rotating frame.

The BCR4BP explicitly depends on time and, therefore, does not possess an integral of the motion. Thus, the energy along the trajectory of *P* is not conserved. However, the instantaneous values of an energy-like quantity offer insights concerning the dynamical flow by exposing instantaneous forbidden regions and instantaneous equilibrium points. This energy quantity is defined in both the E-M rotating frame and the S-B_1 rotating frame, where it is denoted H'. Note that the BCR4BP is periodic. The period, the time interval between two alignments of the Earth, the Moon and the Sun, is denoted the synodic period and is approximately equal to 29.38 days.

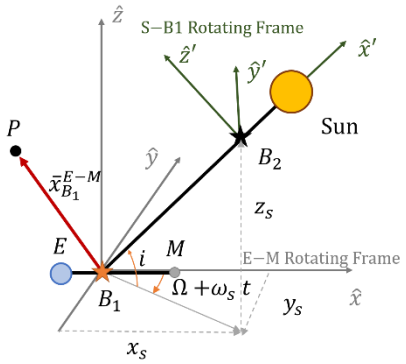

Figure 1. Frames and vector definitions in the BCR4BP

The N-Body Ephemeris Model

For applications in mission scenarios where high-fidelity modeling accuracy is required, N-body differential equations and planetary ephemerides are employed. The N-body dynamics describe the motion of a particle of interest (e.g., a spacecraft) in an inertial frame relative to a central body under the gravitational influence of the same central body and additional perturbing bodies. Within this analysis, the relative position of each perturbing body with respect to the central body is instantaneously computed by employing NAIF SPICE ephemeris data. The Moon is selected as the central body for numerical integration in the J2000 inertial frame. The Earth and Sun are included as point masses, and the Moon's gravity is modeled using the GRAIL (GRGM660PRIM) model truncated to degree and order 8. Solar radiation pressure (SRP) acting on a sphere is also included in the force model.

For multi-revolution propagations in the NRHO prior to a disposal maneuver, orbit maintenance maneuvers (OM maneuvers) are implemented. In some simulations, operational errors on the spacecraft are considered in the higher-fidelity modeling. In these simulations, each OM maneuver is associated with a navigation error on the spacecraft state: both low navigation errors of 1 km in position and 1 cm/s in velocity and larger navigation errors of 10 km in position and 10 cm/s in velocity are considered. Maneuver execution errors comprising 1.5% in magnitude and 1° in direction, as well as a a fixed magnitude of 1.42 mm/s, are applied to each OM maneuver. Mismodeling in SRP assumptions provide 15% error in area and 30% error in coefficient of reflectivity. Momentum wheel desaturations are assumed to occur once per revolution near apolune with a translational Δv component of 3 cm/s applied in a random direction. In addition, the disposal maneuver is either applied error-free (no navigation or execution error considered) or it is applied with a 1.5% execution error and lower or higher navigation errors, as specified in each case. All values are 3σ and are implemented as Gaussian errors with zero mean.

NEAR RECTILINEAR HALO ORBITS IN THE CR3BP, BCR4BP, AND EPHEMERIS MODELS

The southern L_2 halo family bifurcates from a planar Lyapunov orbit and evolves out of plane until the orbits approach the Moon. The NRHO portion of the halo family is defined as the subset of the halo orbits with bounded stability indices.[2] The current investigation focuses on two members of the southern L_2 NRHO family. The first is currently considered the baseline for the primary Gateway orbit; it exhibits a 9:2 resonance with the lunar synodic period. The lunar synodic resonance is attractive for eclipse avoidance applications. By phasing the spacecraft within the NRHO such that perilune passages avoid alignment of the Sun and Earth, long eclipses by the Earth shadow are avoided.[2] The 9:2 lunar synodic resonant NRHO appears in Figure 2a as modeled in the CR3BP. With a perilune radius of approximately 3,250 km and an apolune radius of about 71,000 km, it completes one revolution about every 6.5 days. A second, higher NRHO is in a 4:1 resonance with the lunar synodic period. With appropriate phasing in the 4:1 NRHO, eclipses by the Moon shadow as well as the Earth shadow are avoided.[2] With a longer period of about 7.3 days, the 4:1 NRHO

passes farther from the Moon with a perilune radius of approximately 5,750 km and an apolune radius of about 75,000 km; it appears in Figure 3a. The NRHOs are perfectly periodic in the CR3BP, repeating their behavior at every perilune passage.

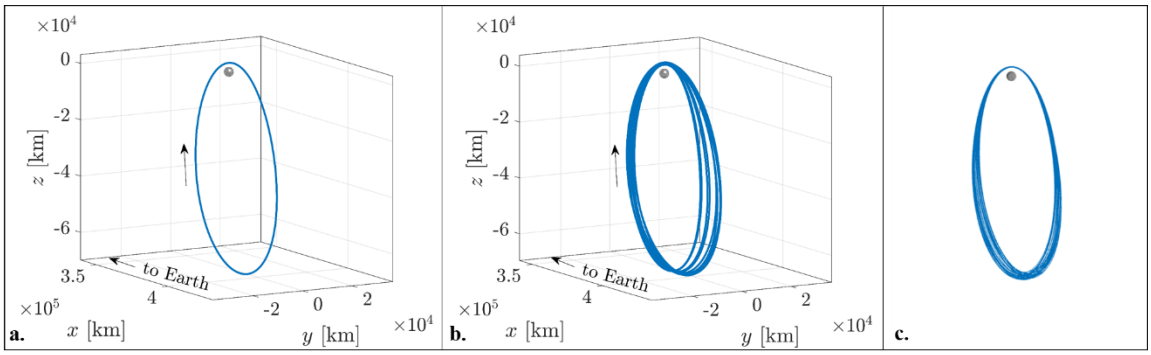

Figure 2. Periodic 9:2 NRHOs in the CR3BP (a) and BCR4BP (b), and quasi-periodic 9:2 NRHO in the ephemeris model (c)

In the BCR4BP, periodic motion is maintained for the CR3BP orbits exhibiting synodic resonance.[6] Generally, for a CR3BP P:Q synodic orbit, periodicity in the BCR4BP is achieved by continuity in position, velocity and Sun angle after P revolutions along the orbit, or equivalently, Q synodic periods. For instance, the 9:2 NRHO has a periodic counterpart in the BCR4BP. Thus, stacking nine revolutions of the 9:2 NRHO in the CR3BP (as in Figure 2a) and correcting for periodicity yields a continuous, periodic trajectory in the BCR4BP. Note that the BCR4BP NRHO repeats every two synodic periods, i.e., about 59 days, while the CR3BP 9:2 NRHO has a period of approximately 6.5 days. That is, the periodic 9:2 NRHO in the BCR4BP, plotted in Figure 2b, repeats after 9 perilune passages, or 2 synodic periods. Similarly, when the 4:1 NRHO is transitioned from the CR3BP (as in Figure 2a) to the BCR4BP, periodicity is maintained. The periodic 4:1 NRHO in the BCR4BP repeats every 4 perilune passages, or each synodic period. Depending solar orientation with respect to the Earth-Moon rotating frame, the characteristics of the periodic 4:1 NRHO vary.

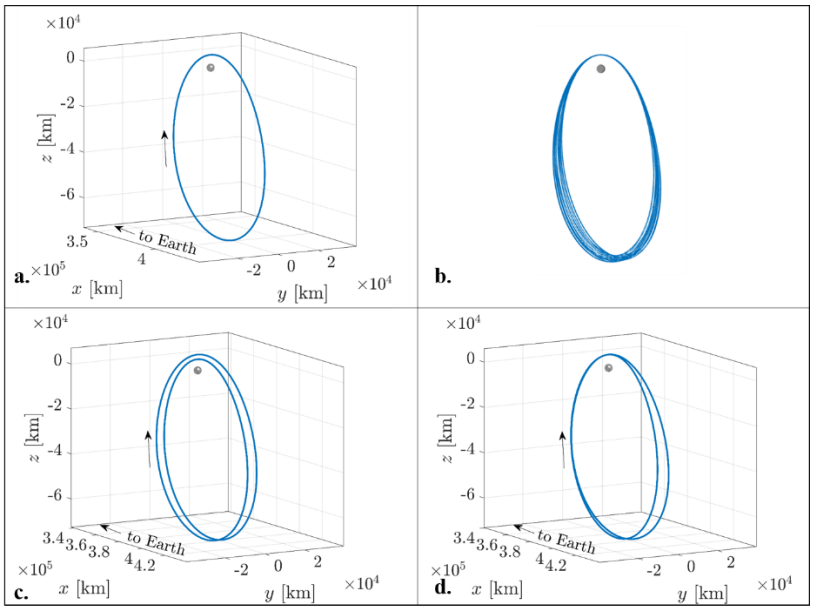

Figure 3. Periodic 4:1 NRHOs in the CR3BP (a) and BCR4BP (c,d), and quasi-periodic 4:1 NRHO in the ephemeris model (b)

For example, two periodic 4:1 NHROs appear in Figures 3c and 3d. In each example, the four lobes of the NRHO cross at a single point; in Figure 4c, the crossing occurs at apolune, while in Figure 4d, the crossing is observed at perilune. Note that at the scale in Figure 4, only two lobes are apparent, but in fact a total of

four lobes are present in each case. It is notable that the 4:1 NRHO in Figure 3c, with the crossing at apolune, is phased to avoid eclipses due to the Earth's shadow, with a Sun angle in multiples of 45°. Conversely, the 4:1 NRHO represented in Figure 3d, whose lobes cross at perilune, is characterized by Sun angles in multiples of 90° and is thus phased such that it experiences eclipses due to the Earth's shadow.

When transitioned to the ephemeris model, the NRHOs evolve into quasi-periodic orbits, maintaining the characteristics of the periodic NRHOs in either the CR3BP or the BCR4BP. These characteristics include stability properties, approximate perilune and apolune radii, and orbital period. A sample 9:2 NRHO in the ephemeris model appears in Figure 2c, while the 4:1 NRHO corrected from CR3BP patch points into the ephemeris force model appears in Figure 3b, with operational errors neglected. In the current analysis, the selected NRHOs are phased to avoid shadows due to the Earth.

Each of the resonant NRHOs is slightly unstable in a linear analysis. Depending on the quality of convergence, an uncontrolled object in either of these NRHOs remains in orbit for an extended time, up to many months. However, the object eventually departs the vicinity of the orbit. Similar behavior is seen in all three dynamical models: while inexpensive orbit maintenance sustains a spacecraft in orbit indefinitely,[7,8] slight instabilities inherent in the NRHOs lead to eventual departure of an uncontrolled spacecraft even without a disposal maneuver.

POST-SEPARATION DYNAMICS AND GATEWAY RECONTACT ANALYSIS

With apolune radii over 70,000 km from the Moon, the 9:2 and 4:1 NRHOs are strongly affected by the gravitational forces of both the Moon and the Earth. Because the NRHOs under consideration for the Gateway are only slightly unstable, an object that separates from the Gateway stack may remain nearby for many revolutions. Until the separated object departs the vicinity of the NRHO, it risks recontacting the Gateway. Thus, it is important to understand the behavior of separated objects within the NRHO vicinity to reduce risk of collision or contamination. Post-separation dynamics depend on the location of the separation along the NRHO as well as on the magnitude and direction of the separation maneuver. The behavior of the departing object varies significantly with even small changes to these parameters, so the design space quickly becomes large. First, the time to depart the NRHO is explored. Then, risk of recontact with the Gateway is considered for varying separation maneuver locations, magnitudes, and directions. While return to the vicinity of the NRHO after initial departure is also a concern, analysis is reserved for a future investigation.

Time to depart the NRHO

To define departure from the NRHO, a momentum integral is employed.[3,6] The momentum integral, MI, is a line integral of the position vector from the initial time, t_0, to the current time, t,

$$\mathrm{MI}(t) = \int_{t_0}^{t} x(\tau)\dot{x}(\tau) + y(\tau)\dot{y}(\tau) + z(\tau)\dot{z}(\tau)d\tau \quad (1)$$

where x, y, and z are components of the position vector relative to the barycenter in the Earth-Moon rotating frame and $\dot{x}, \dot{y},$ and $\dot{z}$ are components of the velocity vector in the same frame. For a perfectly periodic halo orbit in the CR3BP and BCR4BP, the MI is also periodic and returns to zero after each period. In the higher-fidelity ephemeris model, the value of the MI does not return precisely to zero over one period, however, it does remain bounded while the spacecraft remains in the NRHO. Over time, as the orbit of a perturbed or unmaintained spacecraft diverges from the NRHO, the MI also diverges, and departure is defined in terms of the divergence of the MI. For example, consider the curves in Figure 4. The Gateway in a periodic 9:2 NRHO appears in blue as propagated in the CR3BP in Figure 4a; the corresponding periodic MI appears in blue in Figure 4b. A debris object separates from the Gateway with a 1 m/s Δv in the velocity direction at perilune. The resulting trajectory appears in orange in Figure 4a, with the departing MI in orange in Figure 4b. When the magnitude of the MI crosses a threshold of 0.1, the debris object is considered 'departed' from the NRHO. Note that the specific threshold selected to define departure in different applications varies. The range over time between the Gateway and the debris object appears in Figure 4c. Recall that the period of the 9:2 NRHO is about 6.5 days; the regions in the range plot corresponding to local maxima are aligned with perilune passages, while troughs represent apolunes.

Time to depart the NRHO affects two aspects of the current analysis: recontact risk and final destination. For a debris object, cubesat, or larger vehicle departing the Gateway, risk of recontact is assessed while the separated object remains in the NRHO; after departure, the risk of immediate recontact is assumed to cease. In addition, the final destination of the departing object is strongly dependent on the location of the Sun at NRHO departure.[3,9] The time required to depart the NRHO affects the epoch of departure from the NRHO,

and, thus, the orientation of the Sun and final destination of the object. Consistency in time to depart is essential for accurately timing a separation burn to yield a desired post-departure trajectory.

The time between a Gateway separation maneuver and NRHO departure depends on the location, magnitude, and direction of the separation Δ*v*, as well as the selected Gateway NRHO and the choice of MI threshold. It is important to note that the quality of convergence of the numerical Gateway NRHO also impacts the time to escape; a poorly converged Gateway NRHO leads to unrealistically short departure times. The issue of convergence is particularly relevant for analysis in the ephemeris force model, where the Gateway exists in a quasi-periodic NRHO. A well-converged NRHO is necessary for accurate analysis.

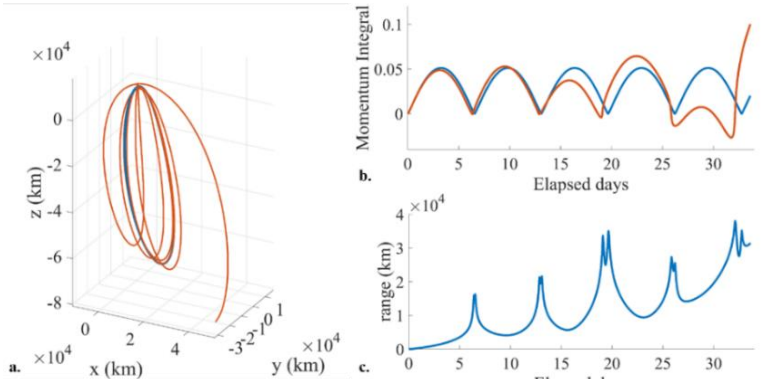

Figure 4. Gateway trajectory (blue) and debris trajectory (orange) in the CR3BP (a). Momentum integrals over time (b). Range between the two objects over time (c).

In general, the larger the separation maneuver magnitude, the faster an object departs the NRHO, with time-to-depart decreasing in discrete steps corresponding to the number of subsequent discrete revolutions around the NRHO. The location along the NRHO that corresponds to the fastest departure time depends on the direction of the separation maneuver. Distinct patterns in departing behavior are apparent when separation maneuvers are aligned with the velocity direction, as well as the directions normal and binormal to the spacecraft velocity along the NRHO. In the current investigation, all three dynamical models (CR3BP, BCR4BP, and ephemeris) are used to assess time to depart and risk of recontact. In the CR3BP and BCR4BP analyses, the velocity direction is defined to be aligned with the spacecraft velocity in the rotating frame, while in the ephemeris model, the velocity direction is aligned with the inertial velocity. These directions differ slightly, but the results remain consistent between the models.

The fastest departures observed from the 9:2 NRHO correspond to a separation burn aligned with the velocity direction near perilune. As the separation location shifts toward apolune, a burn in the velocity direction results in longer departure times. In comparison, a burn aligned normal to spacecraft velocity along the NRHO results in a slower departure from the NRHO, with the longest time to depart corresponding to a burn at perilune. Time to depart the NRHO following a separation maneuver aligned with the binormal direction are relatively consistent regardless of the location of the Δ*v* along the NRHO. Surface plots illustrating the time to depart the 9:2 NRHO for separation burns with magnitude from 0.5 to 15 m/s in the rotating velocity, normal, and binormal (VNB) directions at locations around the NRHO appear in Figure 5 as computed in the CR3BP.

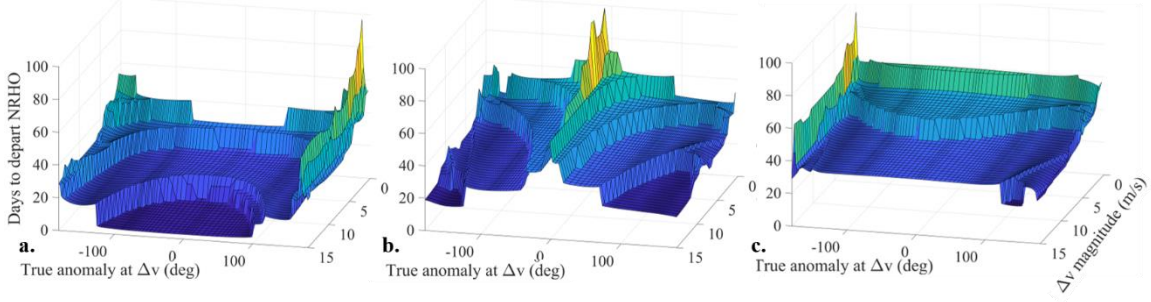

Figure 5. Time to depart the 9:2 NRHO as a function of Δ*v* magnitude and maneuver true anomaly for maneuvers in the rotating velocity direction (a), normal direction (b), and binormal direction (c).

In the CR3BP, each revolution of the periodic NRHO is identical. Thus, a given separation maneuver at a selected location along the NRHO leads to a fixed time to depart. In the BCR4BP and the ephemeris force model, the time to depart the NRHO can vary from revolution to revolution, even if the maneuver itself

(magnitude, direction, and location along the NRHO) is identical. For example, consider the Gateway maintained in a 9:2 NRHO in the ephemeris force model, neglecting navigation, maneuver execution, and other errors. Objects are deployed from the Gateway with identical maneuvers of 1 m/s in the inertial velocity direction at every perilune passage for 50 consecutive revolutions. Each departing object is propagated forward until its momentum integral passes a threshold representing departure from the NRHO, while the Gateway spacecraft is maintained in the NRHO via *x*-axis crossing control.[3] The consistency of time to depart the NRHO between the objects depends on the magnitude of the maneuver and the selected NRHO. The time to depart for objects deployed from a 9:2 and 4:1 NRHO appear in Figure 6 for representative reference trajectories.

Times to depart the NRHO as a function of revolution of the departure burn appear in Figure 6a for the 9:2 NRHO with separation maneuvers of various magnitudes applied to departing objects at consecutive Gateway perilune passages. Note the consistent departure times of ~39 days, or about 6 additional revolutions in the NRHO, for separation maneuvers of 1 m/s. As the Δv magnitude increases, the time to depart decreases in discrete steps corresponding roughly to the period of the NRHO; that is, a separation maneuver of 2 m/s results in departure from the NRHO after ~32 days, or approximately 5 additional revolutions in the NRHO. Consistent times to depart are observed for maneuver magnitudes up to 6 m/s. For burns with magnitudes between 7 and 10 m/s, the time to depart varies depending on which perilune passage is selected for object deployment. The variations are apparent for Δv = 7 m/s and Δv = 9 m/s in Figure 6a, with a distinct pattern visible in the 9 m/s case. While the times to depart vary, they are not random; patterns appear in the data, with behavior tending to repeat after 9 revolutions (2 lunar months) or annually. For Δv magnitudes larger than 10 m/s, the time to depart is again consistent.

In the 4:1 NRHO, similar behavior is observed, but the range of Δv magnitudes that lead to inconsistent, but not random, departure times is wider. Sample cases representing separation burns applied at perilune passages in the 4:1 NRHO appear in Figure 6c. For a small Δv magnitude of 1 m/s, a burn aligned with the Gateway inertial velocity at perilune leads to consistent departure times. For burn magnitudes from 2-9 m/s, variable times to depart are observed as the separation revolution is advanced. For magnitudes of 10 m/s or larger, times to depart are again consistent. Again, patterns appear in the variations in times to depart.

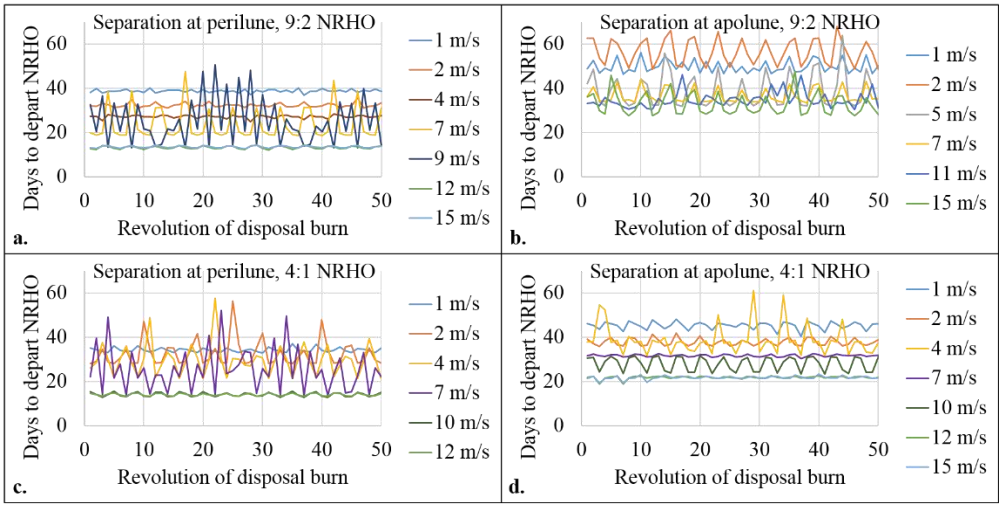

Figure 6. Time to depart the 9:2 NRHO as a function of NRHO revolution. Separation maneuver in the spacecraft inertial velocity direction at perilune in the 9:2 NRHO (a), apolune in the 9:2 NRHO (b), perilune in the 4:1 NRHO (c), and apolune in the 4:1 NRHO (d).

After separation maneuvers in the inertial velocity direction at apolune, objects remain in the vicinity of the NRHO for a longer timespan before departing, and the times to depart are more varied in comparison to burns at perilune. Curves representing time to depart as a function of separation revolution for burns aligned with spacecraft velocity at apolune appear in Figure 6b for the 9:2 NRHO and Figure 6d for the 4:1 NRHO. Objects deploying from the Gateway in the 9:2 NRHO at apolune experience a variable time to depart for separation burns up to 25 m/s. In contrast, consistent times to depart are observed for objects separating from the Gateway in the 4:1 NRHO for Δv magnitudes of 12 m/s and larger. Additionally, for objects departing

the Gateway at apolune in the 4:1 NRHO, lunar impact trajectories are observed for Δv magnitudes of 4 m/s, 9 m/s, and 10 m/s with the selected reference NRHO. However, other patterns may appear with different reference NRHO trajectories. A dynamical explanation for the patterns is sought by employing the BCR4BP.

Inconsistent times to depart from the NRHO are also observed in the BCR4BP model, both for the 9:2 and 4:1 NRHOs. In the 4:1 case, maneuvers at perilune in the rotating velocity direction with magnitude ranging from 2 m/s to 8 m/s yield a varying number of post-maneuver revolutions across the set of initial epochs, that is, across the range of initial Sun angles θ_s. This range of maneuver magnitudes is consistent with the range observed in the higher-fidelity ephemeris model. To explore the dynamical roots of the variation in departure time, a set of 8 periapses from the two periodic 4:1 BCR4BP NRHOs in Figure 4 are sampled. The periapses are separated in epoch by 45° in Sun angle (or equivalently, about 3.68 days), and correspond to the periapses of the two NRHOs plotted in Figures 3c and 3d. Over the range of maneuvers between 1 and 5 m/s, the disposed object completes at least two revolutions before departing from the NRHO. Thus, differentiating patterns are sought between the 'fast' departures, in which the object departs following the minimum amount of time along the NRHO, and the 'slow' departures, which remain in the NRHO for an additional one or two revolutions prior to departure.

The gravitational effects of the Sun on a spacecraft are a function of the Sun-spacecraft relative position. In the equations of motion for the spacecraft expressed in the Earth-Moon rotating frame, the acceleration on the spacecraft due to the Sun is projected on each of the rotating axes such that

$$\bar{a}_S = \begin{bmatrix} a_{S,\hat{x}} \\ a_{S,\hat{y}} \\ a_{S,\hat{z}} \end{bmatrix} = \begin{bmatrix} -m_S \frac{x-x_S}{r_{S3}^3} - m_S \frac{x_S}{r_S^3} \\ -m_S \frac{y-y_S}{r_{S3}^3} - m_S \frac{y_S}{r_S^3} \\ -m_S \frac{z-z_S}{r_{S3}^3} - m_S \frac{z_S}{r_S^3} \end{bmatrix} \tag{2}$$

where m_S is the nondimensional mass of the Sun, r_{S3} is the distance from the Sun to the spacecraft, r_S is the distance from the origin of the Earth-Moon barycenter to the Sun, and x_S, y_S, z_S are the position components of the Sun in the Earth-Moon rotating frame. The integrated effect of the solar gravity, denoted the Sun integral, over the first two revolutions after the execution of the maneuver is defined as

$$S = \int_{t=0}^{T} \|\bar{a}_S\| \, dt \tag{3}$$

where T is the time after two revolutions along the NRHO. Recall that each perilune is sampled along a BCR4BP periodic NHRO, thus converged including the gravitational effects of the Sun. Therefore, the difference between the Sun integral along the disposal trajectory and the Sun integral on the baseline NRHO (with no disposal maneuver) is investigated, rather than solely the Sun integral of the disposal trajectory. The variation in Sun integral is defined as

$$\Delta S_{\%} = 100 \, \frac{S_{\text{disposal}} - S_{\text{baseline}}}{S_{\text{baseline}}} \tag{4}$$

The variations in Sun integral over the range of disposal maneuvers from 1 to 5 m/s appear in Figure 7a, and the corresponding times to depart from the NRHO are plotted in Figure 7b. First, the negative variations in Sun integral yield the fastest departures from the NRHO: these negative variations occur for a Sun angle of -45°, -90°, -215° and -270° relative to the rotating $\hat{x}$ axis. Positive variations in Sun integral also yield departure, but at a slower rate. Second, the magnitude of the maneuver impacts the variation in Sun integral. Increasing the magnitude of the maneuver tends to increase (in absolute value) the variation of Sun integral and, thus, decrease the time to depart from the NRHO. Outliers, for instance, the initial condition of 3 m/s and -315°, are apparent in Figure 7b. Note that the variation in the solar gravitational effect is not the only perturbation affecting the spacecraft during the first two post-maneuver revolutions. The periapses of the BCR4P periodic 4:1 NRHO range from 4,900 km to 7,000 km. Because the dynamical sensitivities are high in this region, small perturbations, including variations in both the solar and lunar gravitational forces on the spacecraft, can generate different types of behavior.

Unless the variations are understood and thus predictable, maneuvers with inconsistent times to departure are not well suited as disposal maneuvers, since the Sun location at departure varies and thus the final destination (heliocentric, Earthbound, or impact) is also inconsistent based on maneuver epoch. It is important to note that in the presence of navigation and maneuver execution errors, the time to depart for small maneuvers can vary significantly even when the error-free case predicts consistent times to depart.[3]

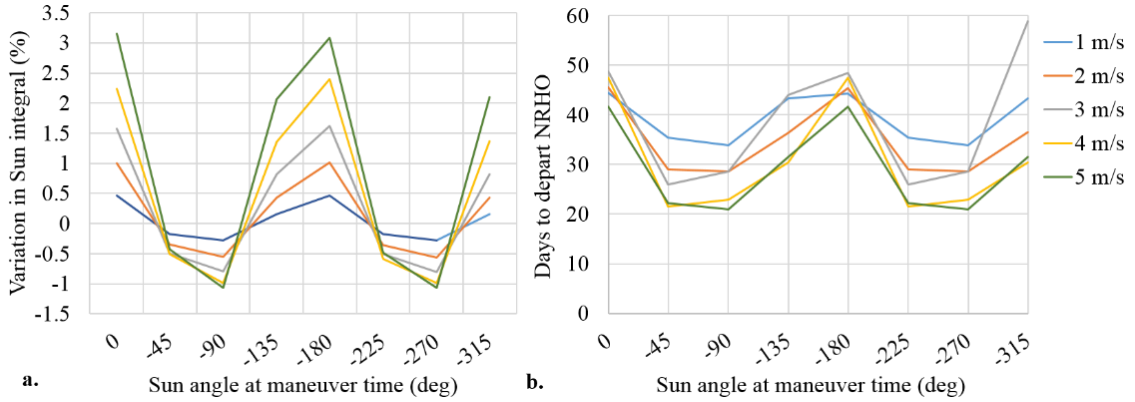

Figure 7. Variation in Sun integral (a) and time to depart (b) as a function of the initial epoch and the magnitude of the disposal maneuver; 1 m/s burn at perilune in the velocity direction.

Gateway range over time

After a spacecraft or debris object has separated from the Gateway but prior to its departure from the vicinity of the NRHO, recontact with the Gateway is a risk. To assess this risk, the range between the Gateway and the departing object is computed for various departure maneuvers. Patterns in the range are apparent when the separation Δv is analyzed in the VNB reference frame. As noted, the magnitude, direction, and location of the separation burn all affect the post-separation behavior. To limit the scope of the design space, recontact risk is investigated in the CR3BP and validated in the ephemeris force model. The analysis is applicable to LMs, cubesats, or small debris objects departing the Gateway. Thus, various magnitudes of Δv are explored.

Consider the Gateway in a 9:2 NRHO, maintained via x-axis crossing control. A separation maneuver aligned with the spacecraft velocity direction (rotating velocity direction in the CR3BP analysis, inertial velocity direction in the ephemeris model) is applied to a series of objects at successive points along a single revolution of the NRHO. The Gateway and the departing objects are propagated forward in time, and the range between the Gateway and each object is computed by differencing their x, y, and z position components and taking the magnitude. A plot of each object's range to the Gateway vs. time as computed in the CR3BP for the 9:2 NRHO appears in Figure 8a for the first 40 days after separation. The x axis represents days past apolune along the 9:2 NRHO; that is, time $t = 0$ represents separation at the first apolune, time $t = 3.25$ corresponds to separation at perilune, and $t = 6.5$ corresponds to separation at the subsequent apolune.

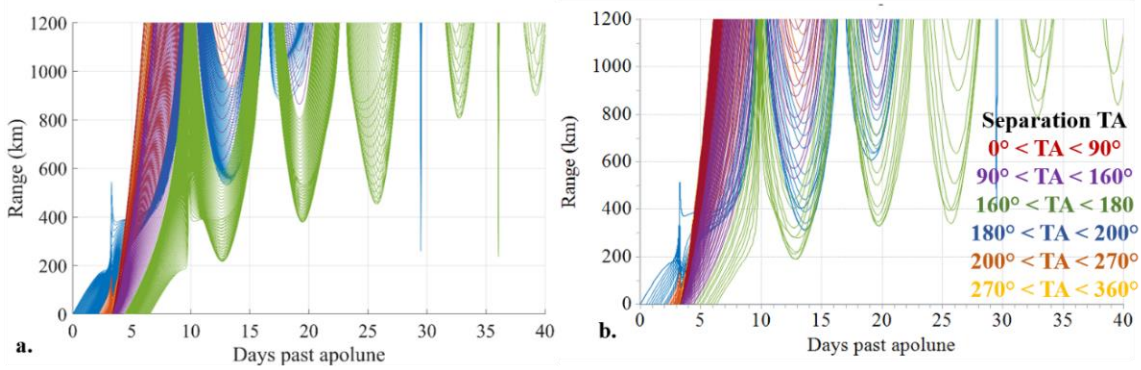

Figure 8. Range to the Gateway over time for objects departing with a 1 m/s Δv in the velocity direction from locations around the 9:2 NRHO in the CR3BP (a) and the ephemeris force model (b).

Each trajectory is colored according to the true anomaly TA along the NRHO at separation according to the legend in Figure 8b. All departing objects start with a range of 0 km as they separate from the Gateway, and the range increases at first as each object moves away. Objects with maneuvers in the velocity direction depart relatively quickly, and recontact risk, defined as a return to a range less than 100 km, is generally low. The main risk of recontact occurs for objects separating from the Gateway shortly after apolune and

encountering the Gateway again at the subsequent perilune passage. Examples appear in blue in Figure 8a. Otherwise, the closest approach after separation is approximately 200km and occurs when an object departs prior to apolune, as seen in green in Figure 8a. The analysis is repeated in the ephemeris force model, neglecting operational errors, and the resulting range plot appears in Figure 8b. While individual trajectories vary, the general behavior closely matches the CR3BP analysis.

The range analysis is performed for separation maneuvers normal to the spacecraft velocity. An object departing after a 1 m/s burn in the normal direction recedes from the Gateway significantly more slowly, and depending on the location of the separation along the NRHO, the object may remain within the 100 km threshold for many revolutions. Examples appear in Figure 9a as propagated in the CR3BP, colored according to the true anomaly at separation as in the legend in Figure 8. Objects separating from the Gateway after apolune with 180° < TA < 270°, represented in blue and orange in Figure 9, risk recontact at the subsequent perilune, but do not return again to the vicinity of the Gateway. Deployment between 90° and 180°, represented in green and purple in Figure B, similarly depart the Gateway without returning within 100 km. However, objects that are deployed immediately before or after perilune with a 1 m/s maneuver in the normal direction demonstrate repeated or continuous risk of recontact, as seen in the red and yellow curves in Figure 9a. The same trends appear when the separation is simulated in the ephemeris force model, as in Figure 9b.

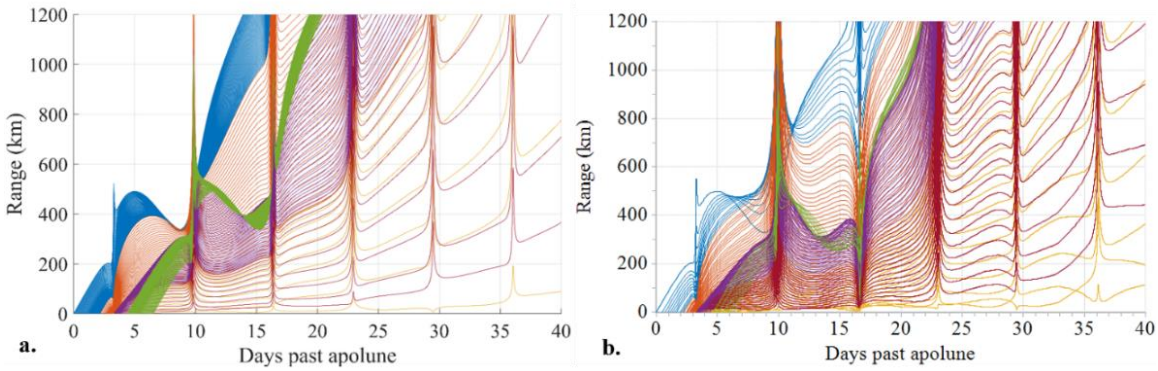

Figure 9. Range to the Gateway over time for objects departing with a 1 m/s Δ*v* in the normal direction from locations around the 9:2 NRHO in the CR3BP (a) and the ephemeris force model (b).

Finally, separation maneuvers in the binormal direction are applied around the 9:2 NRHO, and the range to the Gateway is computed over time. Results from CR3BP analysis appear in Figure 10a, again colored according to separation TA as in the legend in Figure 8. Binormal separation burns from multiple locations along the NRHO lead to recontact risk. Returns to less than 100 km range between 12 and 17 days after the initial apolune are apparent from each region of departure as discretized in the legend in Figure 8. That is, all colors within the plot are seen returning to within 100 km of the Gateway during a 5-day period. Notably, objects that depart from the Gateway when 180° < TA < 200°, represented in blue, return repeatedly to the vicinity of the Gateway.

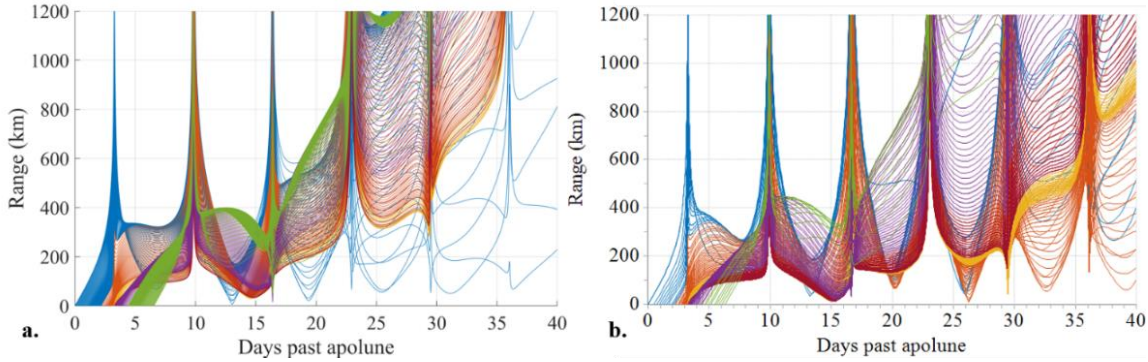

Figure 10. Range to the Gateway over time for objects departing with a 1 m/s Δ*v* in the binormal direction from locations around the 9:2 NRHO in the CR3BP (a) and the ephemeris force model (b).

Results from the analysis in the ephemeris model appear in Figure 10b. Note the differences in the patterns of the range plots after about 17 days of propagation when comparing the CR3BP propagations (Figure 10a) and the ephemeris model propagations (Figure 10b). The epoch of the separation burn determines the solar orientation during the departure. Solar gravity perturbs the departing object, especially as it diverges from the quasi-periodic NRHO, and the location of the Sun determines the nature of the perturbations. The choice of revolution along the Gateway NRHO for the recontact analysis (that is, the precise epoch is represented as time $t = 0$ along the horizontal axis) affects the characteristics of the range plots. Specific selection of the revolution of departure leads to range plots in the ephemeris propagations that match the CR3BP plot very closely. Figure 10b contains a figure that differs from the CR3BP analysis—it is selected to highlight the risk of recontact from objects departing the Gateway with a true anomaly between 200° and 270°. Plotted in orange, these objects repeatedly return to within 100 km of the Gateway at successive apolune passages. These repeated close approaches are not apparent in the CR3BP, and only emerge in the ephemeris model during certain revolutions selected for departure.

The relative velocity between the Gateway and the debris object during periods of close approach varies depending on the location along the orbit where the encounter occurs. For example, consider the set of trajectories represented in Figure 10b. There are several categories of close approaches within this set, that is, regions where the range to the Gateway is less than 100 km. After the initial separation, recontacts occur near perilune passage and near apolune passage for maneuvers in the binormal direction. The first perilune passage in Figure 10b occurs at time $t = 3.25$ days. Subsequent perilune passages occur every 6.5 days. The second ($t = 9.75$ days) and fourth ($t = 22.5$ days) perilune passages of the Gateway do not experience close approaches from any of the departing objects, but the third ($t = 16.25$ days) and fifth ($t = 28.75$ days) perilune passages do see debris objects return to within 100 km of the Gateway. Each apolune passage of the Gateway in the current example experiences debris objects returning to approach the Gateway; apolune passages occur at times $t = 0$ days, $t = 6.5$ days, $t = 13$ days, and so on. The relative velocity as computed in the ephemeris model at every location where the range between the Gateway and a debris object falls below 100 km appears in Figure 11. In the full view in Figure 11a, higher relative velocities are visible at encounters during perilune passages, with values as high as 34 m/s. In the zoomed view in Figure 11b, the lower values of relative velocity are apparent. For every departing object, a range of 0 km at separation is associated with a 1 m/s relative velocity due to the magnitude of the separation burn. For some objects, the relative velocity initially decreases as the range to the Gateway grows immediately after separation. Low relative velocities under 1 m/s are also observed for encounters between 12 and 15 days, prior to perilune at 16.25 days. Then, at each apolune passage prior to departure from the NRHO, some objects return to encounter the Gateway with a relative velocity between 1 and 2 m/s.

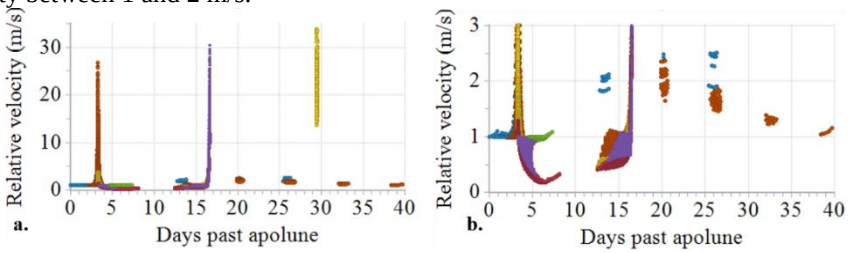

Figure 11. Relative velocity between the Gateway and a debris object for states when the range is less than 100 km for objects represented in Figure 10b. Full view (a) and zoomed view (b).

Figures 8-10 represent the range between the Gateway in the 9:2 NRHO and a departing object for maneuvers of 1 m/s in the velocity, normal, and binormal directions. Such low maneuver magnitudes may represent some types of debris objects and, perhaps, certain small satellites. An increase in the burn magnitude changes the characteristics of the plots. For both the 9:2 and the 4:1 NRHOs, increasing the separation burn magnitude to 5 m/s or higher removes the risk of recontact in the CR3BP for departures in the velocity direction for execution at any location along the NRHO. For burns in the normal or binormal direction, however, risk of recontact remains for Δv magnitudes up to 15 m/s, for particular notable departure locations along the NRHO. For example, range to the Gateway over time for debris objects departing the 4:1 NRHO appear in Figure 12 for four values of Δv magnitude, with colors according to the legend in Figure 8. Note the similarities between Figure 9a, representing a departure Δv of 1 m/s from the 9:2 NRHO and Figure 12a, representing a departure of the same magnitude from the 4:1 NRHO. The patterns observed are very

similar; that is, objects departing immediately before and after perilune, represented in red and yellow, remain near the Gateway for many revolutions. Increasing the burn magnitude to 5 m/s, as in Figure 12b, results in faster departures, but the risk of recontact for objects departing near perilune remains. The same behavior is observed as the separation burn magnitude is increased to 10 m/s (Figure 12c) and 15 m/s (Figure 12d). Objects tend to depart faster with a higher maneuver magnitude, but objects deployed near perilune continue to risk Gateway recontact. It is interesting to note that the patterns observed in Figure 12a, generated with a separation maneuver with Δv = 1 m/s, are almost identically repeated in the other plots in Figure 12 if the scale on the *y* axis is increased 5x, 10x, and 15x, respectively.

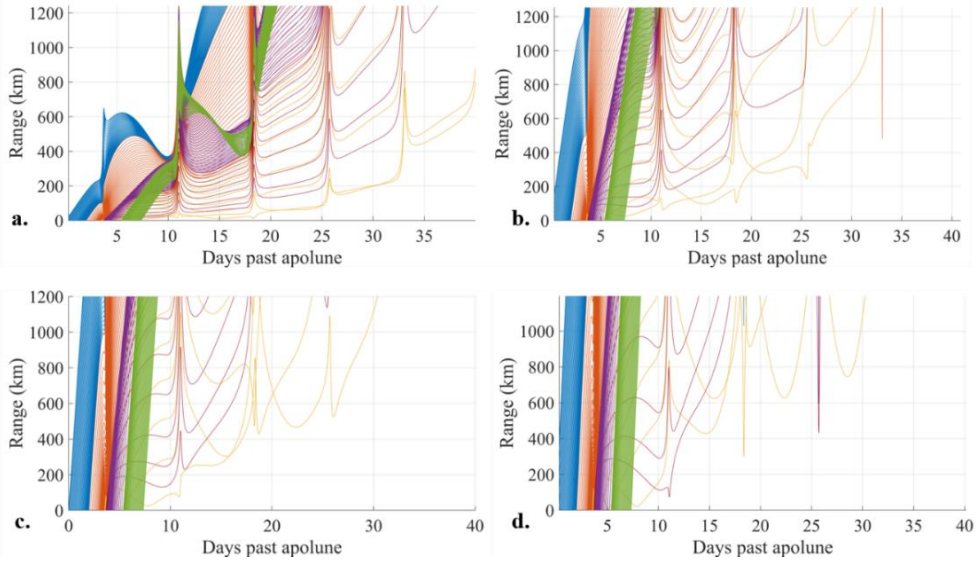

Figure 12. Range relative to the Gateway over time for objects departing in the normal direction from locations around the 4:1 NRHO at 1 m/s (a), 5 m/s (b), 10 m/s (c), and 15 m/s (d)

Figures 8-12 represent behavior after separation burns in the VNB frame. However, some debris objects, for example, particles departing the Gateway from wastewater dumps, are ejected from the Gateway in a body-fixed reference frame. The Gateway is nominally oriented in a tail-to-Sun attitude while Orion is docked and a crew is present.[8] The body-fixed axes of the Gateway are oriented such that the *x* axis is aligned with the long axis of the stack, the *z* axis is aligned with the solar panels and directed towards the celestial southern hemisphere, and the *y* axis completes the right-handed system. Since the NRHO is fixed in the Earth-Moon rotating frame, and the Sun rotates around the frame monthly, the body-fixed axes associated with the Gateway spacecraft rotate through 360° with respect to the NRHO every month. Thus, a burn aligned with the body-fixed frame has components of Δv in each of the V, N, and B directions, and those components change over time. Since the two NRHOs in the current investigation are resonant with the lunar synodic period, the VNB components corresponding to a body-fixed separation maneuver follow approximately repeating patterns. The trajectory behavior after body-fixed separation burns in the 9:2 NRHO repeat every 9 revolutions, and the patterns in the 4:1 NRHO repeat every four revolutions.

To assess risk of Gateway recontact with particles ejected in a particular body-fixed direction, Orion is assumed to be oriented such that the wastewater departs in a body-fixed direction with *x*, *y*, and *z* components defined as [-0.5, 0, 0.866]. Wastewater venting may occur at any time, with a frequency of every three hours while the crew is active. Thus, recontact is assessed for venting at all points around the NRHO. If a body-fixed maneuver is applied at every integration step along the NRHO in the body-fixed frame, the VNB components vary over time. It is thus difficult to characterize a location along the NRHO that is "safe" for a separation in the body-fixed direction. For example, consider an object departing the Gateway from a 4:1 NRHO with a Δv as defined by clocking 1. The range to the Gateway over time for separation locations around the NRHO appear in Figure 13 for two revolutions within the NRHO. The plots are colored according to the legend in Figure 8, so that each color represents a range of true anomaly values at separation. It is clear from Figure 13 that, depending the changing solar orientation, and thus the Gateway attitude, the departure locations that lead to risk of recontact vary from one revolution to the next along the NRHO. The patterns

approximately repeat over time, since in the ephemeris force model the NRHO is quasi-periodic. In the 4:1 NRHO represented in Figure 13, a return to within 100 km of the Gateway appears for separation locations around the NRHO, except for true anomaly values between 90° and 160°.

Figure 13 represents body-fixed separations burns along two revolutions for a single clocking of Orion, a single reference NRHO, and a single Δv magnitude. The characteristics of the plots change when any of these parameters are changed. For example, if the clocking of Orion is rotated, the direction of the body-fixed wastewater vents changes, and the characteristics of the range plots change as well. Similarly, when the phasing of the Gateway within the 4:1 NRHO is adjusted, the separation true anomaly values associated with recontact risk also change. Similar patterns are generated by separation from the Gateway in a 9:2 NRHO; in this case, the patterns approximately repeat every 9 revolutions.

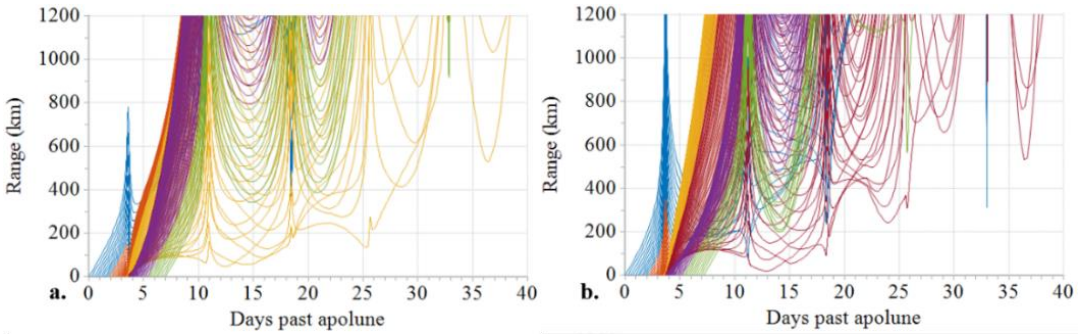

Figure 13. Range to the Gateway over time for objects departing with a 1 m/s Δv in the body-fixed direction from locations along the 4:1 NRHO in the ephemeris model for 2 consecutive revolutions.

The examples thus far assume perfect execution of each separation maneuver. In reality, navigation errors and maneuver execution errors affect deployment, and these errors significantly alter the post-separation behavior. Consider an object separating from the Gateway at a particular location with a selected burn magnitude and direction. The Gateway itself is affected by navigation errors, SRP modeling errors, desaturation perturbations, and errors in the execution of orbit maintenance maneuvers, as described on page 3. At the separation burn, the departing object is subject to navigation errors on its state at departure as well as maneuver execution errors on the separation burn. The extent to which these errors affect the range to the Gateway after deployment depends on the separation maneuver itself. To explore these effects, a Monte Carlo analysis is run in the ephemeris model to compare post-separation behavior in the presence of errors. Two individual separation examples appear in Figure 14. First, an object is deployed from perilune with a separation maneuver in the binormal direction. Recall from Figure 10 that deployment in the binormal direction at 1 m/s leads to recontact for many deployment locations along the NRHO. In the current example, the separation occurs at perilune. A navigation error of 10 km in position and 10 cm/s in velocity (3σ) is assumed during Gateway stationkeeping and at deployment. A 1 m/s maneuver, subject to execution error, is applied at perilune in the binormal direction in 100 Monte Carlo trials, and the range between the object and the Gateway over time for each trial appears in Figure 14a. Despite a single set of values for departure location and deployment maneuver, the range to the Gateway varies considerably. The separation occurs at perilune, at t = 3.25 days. One and a half revolutions later, the Gateway passes through apolune at t = 13 days, and the minimum computed range between the Gateway and the deployed object is 6 km, while the greatest measured range value is 5,500 km. In the presence of errors, the small maneuver leads to unpredictable behavior in the departing object. Increasing the maneuver magnitude to 15 m/s does increase the minimum range at subsequent encounters, but it does not significantly decrease the variance. Results for 100 Monte Carlo trials appear in Figure 14b. In this case, two minima are visible within the first several revolutions, one at t = 11 days and the second at t = 14 days. Close approach range values vary from a minimum of 60 km to a maximum of 5,500 km at the first encounter, and from 300 km to 9,500 km at the second. Similarly, reducing the navigation errors by a factor of 10, to 1 km in position and 1 cm/s in velocity (3σ), does not noticeably reduce the variation in the resulting departing trajectories. However, the errors acting on the spacecraft have a smaller effect for a different set of separation maneuvers. The range to the Gateway over time for a 100-trial Monte Carlo simulation of an object deployed at apolune with a 1 m/s maneuver in the velocity direction, assuming 10 km position errors and 10 cm/s velocity errors (3σ), appears in Figure 14c. Note the difference in scale as compared to the example in Figure 14a. At the subsequent

apolune (t = 6.25 days) the range at the encounter with the Gateway varies by only 70 km, from a minimum of 130 km to a maximum of 200 km. At the second encounter a week later, the range varies between 60 km and 450 km. At perilune 23 days after the separation, the range varies from 25 km to 2,150 km. Increasing the maneuver magnitude to 15 m/s, as in Figure Pd, reduces the variations considerably; the departing trajectories now follow predictable paths with small variations all the way to departure from the NRHO. Similarly, reducing the navigation error by a factor of 10 significantly reduces the variation in the departing trajectories. In summary, in the presence of errors, the predictability of the behavior of departing trajectories depends on the magnitude and direction of the burn, as well as the magnitude of the applied errors.

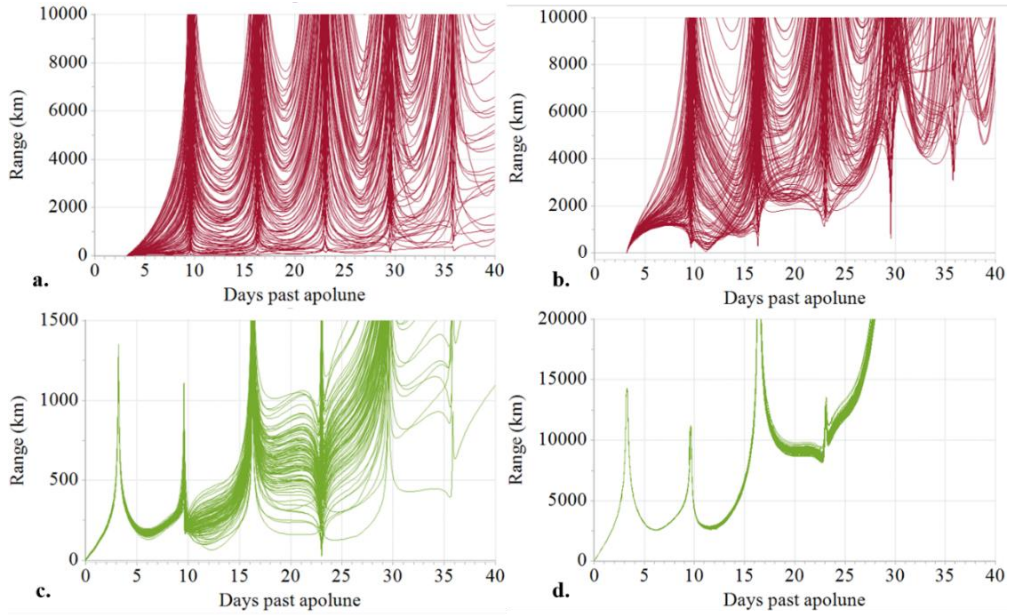

Figure 14. Monte Carlo trials for separation maneuvers in the presence of navigation and maneuver execution errors. Deployment in the inertial binormal direction at perilune at 1 m/s (a) and 15 m/s (b). Deployment in the velocity direction at apolune at 1 m/s (c) and 15 m/s (d).

Recontact Maps

The range plots in Figures 8-10 characterize the departure locations along the 9:2 NRHO where recontact is a risk for a single Δv magnitude and three burn directions. To more completely characterize the design space, a set of recontact maps is generated in the CR3BP. Each map represents departure from a specific location along the NRHO for all possible maneuver directions. A sample map representing deployment from the 9:2 NRHO at a true anomaly TA = 282° with a 5 m/s separation burn appears in Figure 15 on the left. The center of the map represents a maneuver in the rotating velocity direction. The horizontal axis represents maneuver yaw with respect to the velocity vector and ranges from -180° to 180°. The vertical axis represents maneuver pitch with respect to the velocity vector and spans 90° to -90°. Note that in the current investigation, the bottom of the map represents a pitch of 90° while the top of the map corresponds to pitch = -90°. The VNB directions are marked on the map as white points. Green regions in the map represent separation burns that lead to departures without risk of Gateway recontact. Red regions correspond to separation burns that result in recontact risk (range $\leq$ 100 km) prior to NRHO departure. Yellow regions identify separation maneuvers that lead to lunar impact. Sample departing trajectories appear in Figure 15 on the right. The green trajectories depart the NRHO without recontacting the Gateway, with time to depart ranging from approximately 16 to 60 days depending on maneuver direction. The yellow trajectory in Figure 15 originates from the point marked by the crosshairs, representing a maneuver direction with a yaw of -10° and a pitch of -50°. It impacts the Moon prior to departure from the NRHO after a flight time of 48 days. Multiple recontact trajectories are also represented in the map. The red orbits originating from the large, tadpole-shaped red areas in the map risk recontacting the Gateway at the next perilune passage, about 1.5 hours after separation. The red orbits originating from the sine wave-shaped red pattern in the map risk recontacting the Gateway after approximately 34.5 days, or about five revolutions after separation.

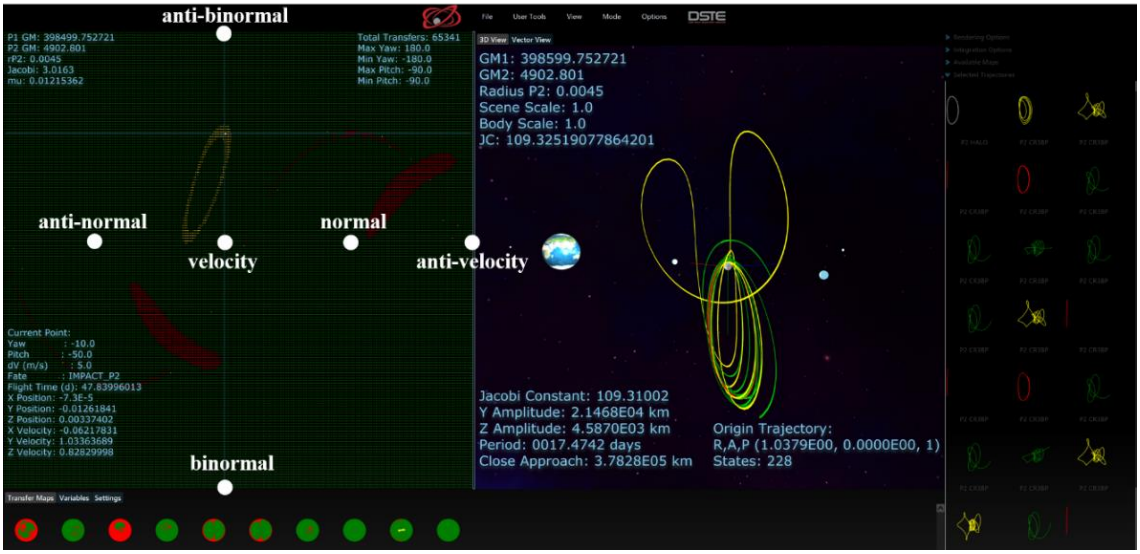

Figure 15. Recontact map and departing trajectories from the 9:2 NRHO.

Recontact maps provide a visual method to quickly assess the risk of recontact or lunar impact for an object separating from the Gateway at a given location and with a particular Δv magnitude in any direction. For the 9:2 NRHO, a set of 15 maps appears in Figure 16. The top row represents departure behavior for a Δv magnitude of 1 m/s for five locations around the NRHO. A Δv magnitude of 1 m/s leads to very limited opportunities for (or risk of) lunar impact. For departure locations between apolune and perilune ($TA \geq 180$) and for $0 \leq TA \leq 140°$, a few yellow points appear in each map. While the points are few, they form distinct patterns. The time of flight between separation and impact generally falls into one of three groups; about 60 days, about 75 days, and about 100 days. For departure locations between perilune and apolune ($140 < TA < 180$), no yellow points appear on the maps; thus, there is no maneuver direction for which a 1 m/s burn leads to lunar impact for such separation locations. Risk of recontact, represented by red regions on the map, occurs for a wide range of maneuver directions, especially for separation after apolune, $180° < TA < 282°$. Depending on the location and direction of the separation, the time of flight between separation and recontact can range from a few hours to several weeks.

When the separation Δv magnitude is increased, the characteristics of the recontact maps change. The center row in Figure 16 consists of maps representing departure from the 9:2 NRHO with a 5 m/s separation burn. The larger separation burn reduces the risk of recontact and increases the risk of (or opportunity for) lunar impact. The risk of recontact does not disappear, however. For certain maneuver directions, separation after apolune where $200° \leq TA \leq 280°$ leads to recontact risk at the next perilune with a 5 m/s burn. However, recontacts after long times of flight are rare with a 5 m/s burn. In contrast, maneuver options for lunar impact are more widespread. For example, a range of burn directions centered on the anti-velocity direction at perilune result in lunar impact, as seen by the two yellow half circles in the map corresponding to $TA = 0°$.

Increasing the Δv magnitude further to 15 m/s again reduces the risk of recontact and opportunities for lunar impact. A set of maps corresponding to 15 m/s separation maneuvers appears in the bottom row of Figure E. Red regions still exist in the maps; departures between apolune and perilune result in recontact risk at the subsequent perilune for certain maneuver directions. However, recontact is not a risk for departure from locations corresponding to $TA < 180°$. Yellow regions in the maps, representing maneuver directions that lead to impact, are observed centered on the anti-velocity direction near perilune and the anti-binormal direction between apolune and perilune. Departures from apolune rarely lead to lunar impact regardless of maneuver direction for separation maneuvers up to 15 m/s in magnitude.

A similar set of recontact maps is generated for the 4:1 NRHO in the CR3BP; while details vary, the same types of patterns are present. That is, for maneuver magnitudes of 1 m/s, risk of recontact is widespread for separation between apolune and the following perilune passage, but lunar impact is rare. For higher separation Δv values, the regions on the maps that lead to lunar impact expand, but with a higher starting perilune radius, separations from the 4:1 NRHO lead to fewer lunar impact trajectories as compared to the 9:2 case.

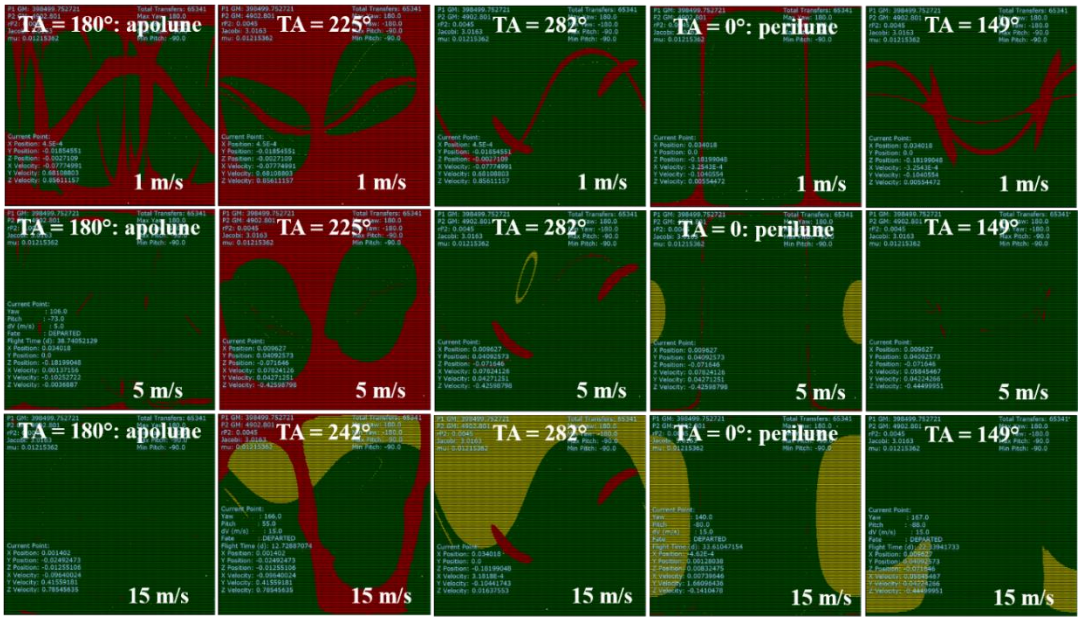

Figure 16. Recontact maps for the 9:2 NRHO. Five departure locations around the NRHO, Δ*v* magnitude of 1 m/s (top), 5 m/s (center), 15 m/s (bottom). Recontact threshold: 100 km.

The characteristics of lunar impact trajectories vary significantly based on the maneuver magnitude and direction. Six examples of impact orbits that depart from the 9:2 NRHO appear in Figure 17. The times of flight between separation and impact vary from 10 days for the orbit in Figure 17a, which separates from the Gateway with a 15 m/s Δ*v* at perilune, to 110 days for the trajectory in Figure 17f, with a 1 m/s separation at perilune. In Figure 17b, a 5 m/s departure at perilune impacts the Moon after 23 days. In Figure 17c, a 1 m/s maneuver at apolune leads to impact after 60 days and a large loop around the Moon, while in Figure 17d, following a 5 m/s separation at TA = 225°, a trajectory achieves lunar impact after 63 days and an excursion to a northern family of orbits. In Figure 17e, the departing object impacts the Moon 70 days after a separation Δ*v* of 1 m/s at perilune. Note the symmetry in the impact trajectories appearing in Figures 17e and 17f. Both depart the Gateway at perilune with a magnitude of 1 m/s, but in different maneuver directions. A discussion of lunar impact locations and velocities is reserved for a future study.

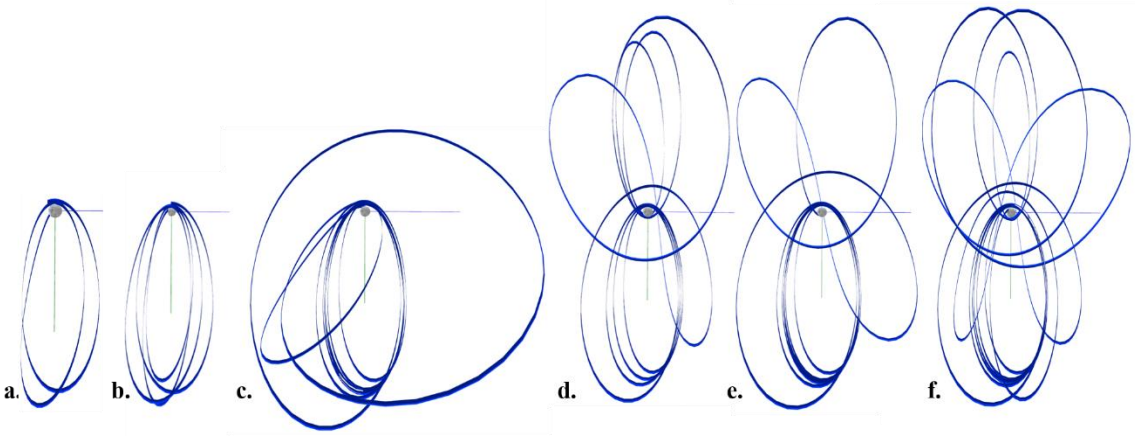

Figure 17. Lunar impact trajectories in the CR3BP.

To fully explore the design space, recontact maps are generated for many locations along both the 4:1 and 9:2 NRHOs and for a list of values of Δ*v* magnitude. To reduce the time required to generate the maps, the Java-based Deep Space Trajectory Explorer[12] is employed for map generation and analysis. A specialized "Recontact Integrator" is extended from the existing DSTE Runge-Kutta 7-8 adaptive step integrators to

propagate multiple objects: an origin trajectory and N objects that separate from the origin. Separations are modeled as maneuvers from the origin trajectory, and the range is recorded to the origin spacecraft as well as both central bodies. A user interface provides range and step size inputs for the yaw, pitch, Δv magnitude, and origin state. At each time along the adaptive step integration, the Recontact Integrator performs event detection logic-based comparisons of the separation states back to the origin trajectory. As an event is detected, the fate is determined for the separated object. To determine if an object has departed, the momentum integral is accumulated at each adaptive step. If the momentum integral passes a user defined threshold, the transfer is considered departed. A transfer is considered to have recontacted the origin trajectory if at any point during the integration 1) the position of the separated object is inside a user defined distance threshold and 2) the current range is not increasing. Finally, a separation transfer is considered an impact if the range to the surface of any of the bodies of the system, in this case the Earth and the Moon, becomes negative. The order of priority for the event detection is body impact, departure, and then recontact.

The fate of each trajectory is captured and exported as both a data file and a visual recontact map. The DSTE automatically separates map generation using the origin state as the logical demarcation. Logical separation in this manner facilitates broad simulations that can span any possible range of departures from a given origin trajectory. To accelerate the computations, the DSTE automatically executes recontact integration for each separation transfer combination in parallel using the Java Parallel Streams API and all available cores. For input ranges that are exhaustively large, the DSTE Cloud Service provides a highly scalable recontact integration capability that can be optionally connected to via the user interface. As the computations are completed, the results and fate of each separation transfer are asynchronously transferred to and visualized as a Recontact Map shown in previous figures.

DEPARTURE DYNAMICS TO HELIOCENTRIC DISPOSAL

Escape to heliocentric space, defined here as the region beyond the Sun-B_1 L_1 and L_2 libration points, is a potential option for the disposal of logistics modules and other objects from the Gateway. Direct escapes are defined by immediate transit from the NRHO to heliocentric space, while indirect escapes are characterized by additional revolutions around the Earth-Moon barycenter prior to achieving heliocentric escape. Failures are defined as trajectories that do not escape to heliocentric space in one year, impact one of the primaries, or enter the Earth-Moon vicinity, that is, the sphere centered at the Earth-Moon barycenter of radius equal to the Earth-Moon L_1 distance. The success or failure of an attempted escape to heliocentric space depends on the orientation of the Sun and the energy of the trajectory with respect to the Sun-B_1 system as the spacecraft departs a 9:2 NRHO.[3] Similar results characterize escape from a 4:1 NRHO. Recall that inconsistent times to depart from the 4:1 NRHO are observed for maneuvers at perilune in the velocity direction with magnitudes from 2 to 9 m/s. That is, various numbers of post-maneuver revolutions prior to NRHO departure result in different Sun-Earth-Moon-debris configurations at the departure time. This inconsistency complicates the disposal problem. Thus, velocity-direction maneuvers of magnitude of 1 m/s and 15 m/s, both of which yield consistent times to depart the 9:2 and 4:1 NRHOs when applied at perilune, are considered in both the BCR4BP model and the ephemeris force model.

In the BCR4BP, disposals from the two periodic 4:1 NRHOs appearing in Figures 4c and 4d are considered. Each of the two NRHOs possesses four distinct perilune locations in the Sun-Earth frame. The eight individual perilune locations are candidates for separation maneuvers; they are separated in epoch by approximately 3.68 days, or equivalently, 45° in Sun angle. These eight periapses form a representative subset of the Earth-Moon-Sun-spacecraft configurations over a synodic month. For a disposal maneuver of 1 m/s, no successful disposal is observed. The trajectories that re-enter the Earth-Moon vicinity are plotted in Figure 18. For clarity purposes, the captures, i.e., the trajectories that do not escape the Earth-Moon vicinity, are not included in the figure; they correspond to initial Sun angles of -45°, -135°, -225° and -315°. The trajectories plotted in Figure 18 do escape to heliocentric space but are not considered successful outcomes in this investigation, since the debris re-enters the Earth-Moon vicinity. Note that the locations of the apses with respect to Earth-Moon barycenter in Figure 18b and the geometry of the trajectory are consistent with the tidal acceleration from the Sun.[10] The energy-like quantity along the trajectory in the Sun-B_1 rotating frame, the Hamiltonian H', is plotted as a function of time past the disposal maneuver in Figure 18c. The black lines represent the instantaneous Hamiltonian of the Sun-B_1 portals L_1 and L_2 in the BCR4BP. Note that L_1 and L_2 have distinct values, but they are indistinguishable at this scale. Above the black line, the energy along the trajectory is too low to allow transit through the portals. Below this line, both portals are

open and disposal to heliocentric space is possible. In contrast, 1 m/s velocity-direction burns do lead to direct escapes from the 9:2 NRHO.[3]

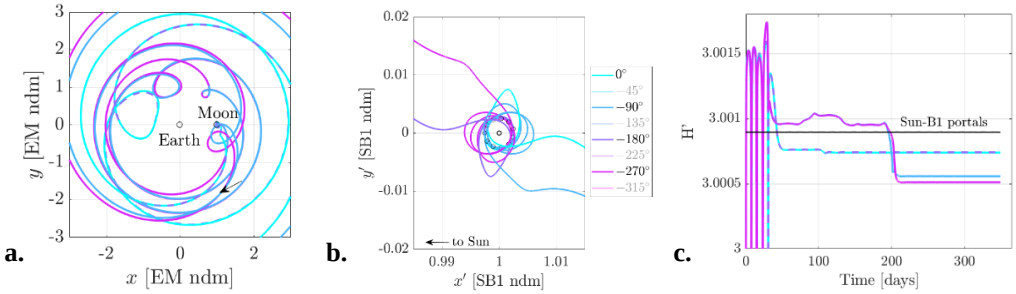

Figure 18. Trajectories for a disposal maneuver of 1 m/s from the BCR4BP 4:1 NRHO, as seen in the Earth-Moon rotating frame (a) and the Sun-B_1 rotating frame (b). Sun-B_1 Hamiltonian along the trajectory (c).

For a disposal maneuver of 15 m/s, six out of the eight initial Sun angles result in escape to heliocentric space in the BCR4BP, as seen in Figure 19. Trajectories that re-enter the Earth vicinity are observed for separation maneuvers at Sun angles of 0° and -180°, and are, thus, considered unsuccessful disposals. Separation maneuvers at the other six Sun angles result in direct escape to heliocentric space. In each case, the energy at the time of departure is high enough such that the Sun-B_1 portals are open, seen in Figure 19c. By appropriately phasing the epoch of the maneuver with the Sun, direct escapes to heliocentric space are achieved for 15 m/s maneuver magnitudes.

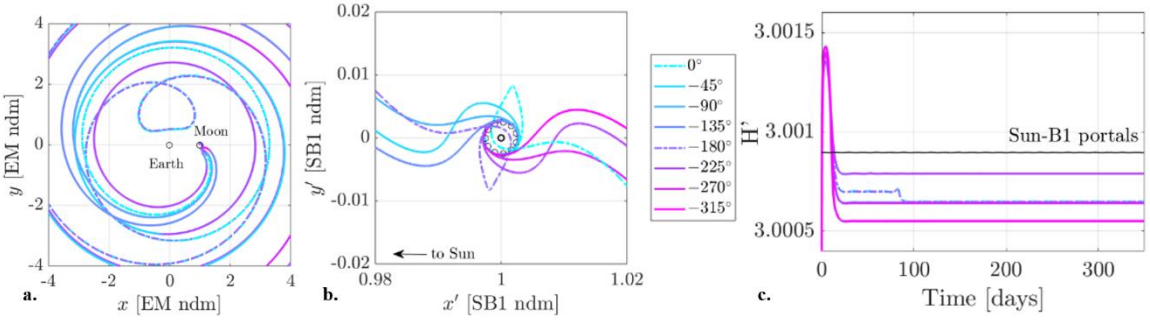

Figure 19. Direct escape for a disposal maneuver of 15 m/s, as seen in the Earth-Moon rotating frame (a) and the Sun-B1 rotating frame (b). Sun-B1 Hamiltonian along the trajectory (c).

The disposal analysis is also conducted for the periodic BCR4BP 9:2 NRHO. The 9:2 NRHO performs nine revolutions around the Moon before returning to the same state in both position and velocity. In the meantime, the Sun, as observed from the Earth-Moon rotating frame, performs two revolutions around the Earth-Moon barycenter. Thus, the perilune passages of the BCR4BP 9:2 NRHO are separated in epoch by approximately 6.5 days, or equivalently, 80 degrees of the Sun angle. Similar to the analysis performed for the periodic BCR4BP 4:1 NRHO, a disposal maneuver is performed at perilune, in the direction of the rotating velocity. The locations of the maneuver in the Sun-B_1 rotating frame are plotted in Figures 20b and 20c. Maneuvers marked in red lead to heliocentric escape; blue maneuvers lead to earthbound trajectories. A set of quadrants defined in a counterclockwise fashion in the Sun-B_1 rotating frame facilitate the interpretation of the plots. For maneuvers of 1 m/s, implementing the disposal maneuver at an apolune located in quadrants II and IV leads to heliocentric escape. A band of initial conditions located in quadrants I and III result in earthbound trajectories. The pattern of escape does not vary significantly when increasing the disposal maneuver magnitude to 15 m/s, as seen in Figure 20d. While the phasing of the Sun is similar for escapes at 1 and 15 m/s, the trajectories are different: for instance, the objects depart from the NRHO much faster at 15 m/s than 1 m/s. Maneuver plots are also created for the periodic BCR4BP 4:1 NRHO, using the trajectory data plotted in Figures 17 and 18, and appear in Figures 20a and 20c. Certain locations are preferable to depart from the 4:1 or the 9:2 NHRO to reach heliocentric space. The locations are function of the orbit to be disposed from and the magnitude of the disposal maneuver.

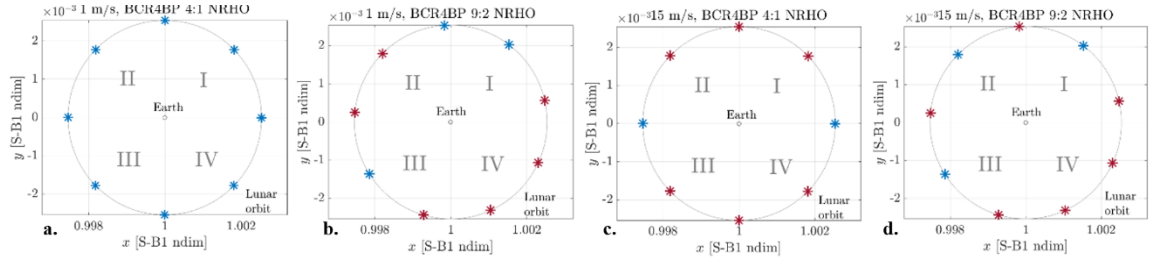

Figure 20. Separation maneuver location in the Sun-B_1 rotating frame. 1 m/s separation at perilune of a 4:1 (a) and a 9:2 NRHO (b). 15 m/s separation at perilune of a 4:1 (c) and a 9:2 NRHO (d).

A similar analysis is performed in the ephemeris force model. Patch points from the 4:1 NRHO in the CR3BP are stacked and corrected into a continuous NRHO in the ephemeris model;[11] by changing the epoch of the patch points, the Sun angle at the initial perilune is varied. A set of 15 reference NRHOs in the ephemeris model is generated with starting epochs ranging from May 1-15, 2023 and Sun angles at perilune ranging from 0° to -360°. Similarly, 15 9:2 NRHOs are generated in the ephemeris model with epochs spanning May 2-30, 2023. Neglecting navigation and spacecraft errors, separation maneuvers aligned with inertial spacecraft velocity are applied at each perilune passage for 50 revolutions in each reference NRHO; that is, 750 separate separation maneuvers are sampled for both the 4:1 NRHO and the 9:2 NRHO, and each deployed object is propagated forward for 100 days. An object is considered escaped to heliocentric space if it lies outside the Sun-B_1 L_1 and L_2 libration points at the end of the 100-day propagation. In general, this 100-day limit selects for direct escapes from the Earth-Moon vicinity. Extending the propagation time additionally identifies indirect escape trajectories; however, for reliable disposal of logistics modules or other objects, direct escapes are preferable. After each propagation, the fate of the separated object is recorded; heliocentric escapes are marked in red and earthbound objects in blue on the maps in Figure 21. The position of each point represents the location of the separation maneuver at perilune in the Sun-Earth rotating frame. In the ephemeris force model, none of the 750 sampled separation burns of 1 m/s in the velocity direction achieve a high enough energy H' to escape from the Earth-Moon vicinity within 100 days; the map in Figure 21a is entirely blue. This is in distinct contrast to the 9:2 NRHO case,[3] which experiences direct escape for 1 m/s velocity-direction separation maneuvers from a majority of Sun angles, shown here in Figure 21b. When the Δv is increased to 15 m/s, as predicted by the BCR4BP analysis, escapes from the 4:1 NRHO within 100 days occur for all separation maneuvers not located near the Sun-B_1 x-axis, as in the map in Figure 21c. That is, only Sun angles centered around 0° and -180°, the two angles leading to indirect escape in the BCR4BP analysis, fail to lead to escapes in less than 100 days in the ephemeris model. Escapes from the 9:2 NRHO with a magnitude of 15 m/s in the velocity direction show similar behavior, as is apparent in the map in Figure 21d, though the blue regions corresponding to earthbound trajectories shifted slightly on the map. The ephemeris model results in Figure 21 agree with BCR4BP analysis in Figure 20.

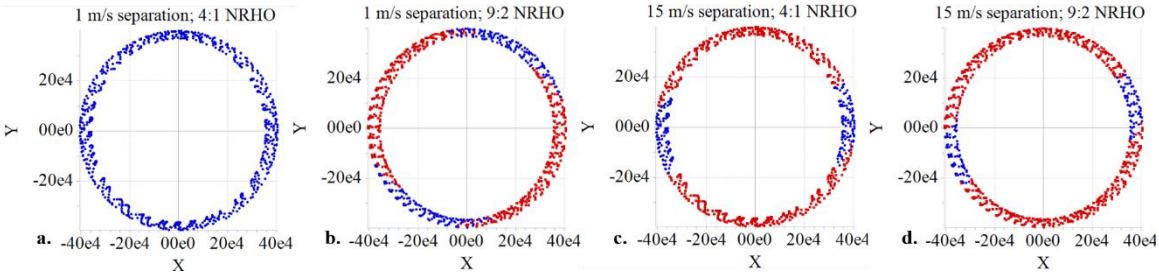

Figure 21. Separation maneuver location in the Sun-B_1 rotating frame. 1 m/s separation at perilune of a 4:1 (a) and a 9:2 NRHO (b). 15 m/s separation at perilune of a 4:1 (c) and a 9:2 NRHO (d).

Recall that small separation maneuvers lead to unpredictable post-separation behavior when errors on the spacecraft and the maneuver are considered, as illustrated in Figure 14. In a Monte Carlo analysis, escape to heliocentric space is not reliable, even when separation occurs at a favorable Sun angle in the 9:2 NRHO.[3] For departure from either of the resonant NRHOs, a 15 m/s maneuver is more appropriate for reliable escape to heliocentric space.

SUMMARY AND CONCLUDING REMARKS

The Gateway is planned to orbit in an NRHO within the multibody dynamical environment of cislunar space. Various objects, including cubesats, logistics modules, and debris particles, are expected to depart from the Gateway with relatively small separation maneuvers. The current investigation explores several aspects of the dynamics of departure from the NRHO. Three dynamical models are employed: the CR3BP effectively describes the behavior of an object immediately after separation from the NRHO; the BCR4BP extends the effectiveness of a simplified model beyond the NRHO by including solar gravity; and a higher-fidelity ephemeris model offers accurate descriptions of trajectory behavior but also complicates the analysis. In both the CR3BP and the BCR4BP, the 9:2 and 4:1 NRHOs are perfectly periodic.

Time to depart the NRHO based on maneuver magnitude, location, and direction is explored in the CR3BP, where the fastest departures occur after separation maneuvers in the velocity direction at perilune. In the BCR4BP and the ephemeris model, such maneuvers result in variable time to depart for maneuver magnitudes. The range between the Gateway and a departing object is explored to assess risk of recontact. Patterns in the post-separation range appear when the maneuvers are defined in the VNB frame. Maneuvers in the velocity direction offer opportunities for departure without recontact. For some departure locations around the NRHO, a small separation burn in the direction normal to the NRHO leads to multiple revolutions with repeated recontact risk. An object deployed from the Gateway with a 1 m/s maneuver in the binormal direction in nearly any location around the NRHO risks recontact at a later date. If an object is ejected from the Gateway with a Δv in the body-fixed frame, the trajectory behavior depends on the epoch of deployment, phasing within the NRHO, and clocking of the ejection. Recontact maps are generated to condense the large design space and provide an intuitive visual method for determining the risk of recontact for an object deployed with a given separation maneuver. After departure from the NRHO, some applications call for escape to heliocentric space. The 9:2 NRHO offers escape opportunities for maneuvers of both 1 m/s and 15 m/s magnitude, given a favorable Sun orientation at the maneuver. Direct escape from 4:1 NRHO is not available for a 1 m/s burn in the velocity direction, but raising the separation burn magnitude to 15 m/s yields heliocentric escape for most Sun orientations. In either NRHO, the 15 m/s magnitude burn leads to significantly more reliable escape options in the presence of spacecraft and navigation errors.

ACKNOWLEDGMENTS

The authors would like to thank Ryan Whitley for his insight and assistance. Portions of this work were completed at NASA JSC and Purdue University through contract #NNJ13HA01C and grant #NNX13AK60A, respectively.

REFERENCES

[1] Gates, M., M. Barrett, J. Caram, V. Crable, D. Irimies, D. Ludban, D. Manzell, and R. Ticker, "Gateway Power and Propulsion Element Development Status," 69th International Astronautical Congress, Bremen, Germany, October 2018.

[2] Zimovan, E., K. C. Howell, and D. C. Davis, "Near Rectilinear Halo Orbits and Their Application in Cis-Lunar Space," 3rd IAA Conference on Dynamics and Control of Space Systems, Moscow, Russia, May-June 2017.

[3] Boudad, K. K., D. C. Davis, and K. C. Howell, "Disposal Trajectories From Near Rectilinear Halo Orbits," AAS/AIAA Astrodynamics Specialists Conference, Snowbird, Utah, August 2018.

[4] Szebehely, Z., *Theory of Orbits: The Restricted Problem of Three Bodies*, Academic Press, New York, 1967.

[5] Gomez, G., J. Llibre, R. Martinez, and C. Simo, *Dynamics and Mission Design near Libration Points*, Vol. 2. World Scientific, 2001.

[6] Boudad, K., "Disposal Dynamics from the Vicinity of Near Rectilinear Halo Orbits in the Earth-Moon-Sun System", M.S. Thesis, December 2018, West Lafayette, Indiana.

[7] Guzzetti, D., E. M. Zimovan, K. C. Howell, and D. C. Davis, "Stationkeeping Methodologies for Spacecraft in Lunar Near Rectilinear Halo Orbits," AAS/AIAA Spaceflight Mechanics Meeting, San Antonio, Texas, February 2017.

[8] Newman, C. P., D. C. Davis, R. J. Whitley, J. R. Guinn, and M. S. Ryne, "Stationkeeping, Orbit Determination, and Attitude Control for Spacecraft in Near Rectilinear Halo Orbits," AAS/AIAA Astrodynamics Specialists Conference, Snowbird, Utah, August 2018.

[9] Bucci, L., A. Kleinschneider, M. Lavagna, and F. Renk, "Optimal Escape Manifolds for Cis-Lunar Halo Orbits," 69th International Astronautical Congress, Bremen, Germany, October 2018.

[10] Davis, D.C., Multi-body Trajectory Design Strategies Based on Periapsis Poincaré Maps. PhD Dissertation, Purdue University, 2011.

[11] Davis, D.C., S. M. Philips, K. C. Howell, S. Vutukuri, and B.P. McCarthy, "Stationkeeping and Transfer Trajectory Design for Spacecraft in Cislunar Space," AAS/AIAA Astrodynamics Specialist Conference, Stevenson, Washington, August 2017.

[12] Davis, D.C., S. M. Phillips, and B.P. McCarthy, "Trajectory Design for Saturnian Ocean Worlds orbiters using multidimensional Poincaré maps," *Acta Astronautica*, November 2017.